Cbl and Cbl-b independently regulate EGFR through distinct receptor interaction modes

Itziar Pinilla-Macua* and Alexander Sorkin
Department of Cell Biology, University of Pittsburgh, School of Medicine, Pittsburgh, PA, 15261

ABSTRACT **Highly homologous E3 ubiquitin ligases, Cbl and Cbl-b, mediate ubiquitination of EGF receptor (EGFR), leading to its endocytosis and lysosomal degradation. Cbl and Cbl-b, are thought to function in a redundant manner by binding directly to phosphorylated Y1045 (pY1045) of EGFR and indirectly via the Grb2 adaptor. Unexpectedly, we found that inducible expression of Cbl or Cbl-b mutants lacking the E3 ligase activity but fully capable of EGFR binding does not significantly affect EGFR ubiquitination and endocytosis in human oral squamous cell carcinoma (HSC3) cells which endogenously express Cbl-b at a relatively high level. Each endogenous Cbl species remained associated with ligand-activated EGFR in the presence of an overexpressed counterpart species or its mutant, although Cbl-b overexpression partially decreased Cbl association with EGFR. Binding to pY1045 was the preferential mode for Cbl-b:EGFR interaction, whereas Cbl relied mainly on the Grb2-dependent mechanism. Overexpression of the E3-dead mutant of Cbl-b slowed down EGF-induced degradation of active EGFR, while this mutant and a similar mutant of Cbl did not significantly affect MAPK/ERK1/2 activity. EGF-guided chemotaxis migration of HSC3 cells was diminished by overexpression of the E3-dead Cbl-b mutant but was not significantly affected by the E3-dead Cbl mutant. By contrast, the inhibitory effect of the same Cbl mutant on the migration of OSC-19 cells expressing low Cbl-b levels was substantially stronger than that of the Cbl-b mutant. Altogether, our data demonstrate that Cbl and Cbl-b may operate independently through different modes of EGFR binding to jointly control receptor ubiquitination, endocytic trafficking, and signaling.**

SIGNIFICANCE STATEMENT

- Highly homologous E3 ubiquitin ligases, Cbl and Cbl-b, mediate ubiquitination of EGF receptor (EGFR), leading to its endocytosis and lysosomal degradation. Cbl and Cbl-b are thought to function in a redundant manner by binding directly and indirectly to activate EGFR.
- Here, we demonstrate that Cbl and Cbl-b may operate independently through different modes of EGFR binding to jointly control receptor ubiquitination, endocytic trafficking and motility signaling in oral squamous cell carcinoma cells.
- Inhibition of Cbl and Cbl-b has the potential to be developed as a therapeutic approach for preventing metastatic growth of EGFR-dependent tumors.

Monitoring Editor
Avery August
Cornell University

Received: Feb 15, 2023
Revised: Sep 22, 2023
Accepted: Oct 11, 2023

This article was published online ahead of print in MBoC in Press (http://www.molbiolcell.org/cgi/doi/10.1091/mbc.E23-02-0058) on October 30, 2023.
Competing financial interests: None.
*Address correspondence to: Itziar Pinilla-Macua (itp2@pitt.edu).
Abbreviations used: Cbl, Casitas B-lineage lymphoma; CME, clathrin mediated endocytosis; Dox, doxycycline; EGF, epidermal growth factor; EGFR, EGF receptor; RTK, receptor tyrosine kinase; ERK1/2, extracellular signal-regulated kinase 1/2; TGH, Triton X-100-glycerol-HEPES; TKB, tyrosine kinase binding; UBA, ubiquitin associated.

INTRODUCTION

Epidermal growth factor (EGF) receptor (EGFR) is an archetypal member of the receptor tyrosine kinase (RTK) family. EGFR is essential for mammalian development and tissue homeostasis in adult organisms (Sibilia *et al.*, 2007; Pastore *et al.*, 2008). EGFR is mutated or overexpressed in various types of cancer and has become the major therapeutic target and prognostic marker (Uribe *et al.*, 2021). Ligand binding to EGFR at the cell surface triggers activation of the tyrosine kinase in the receptor cytoplasmic domain and tyrosine phosphorylation of the receptor itself and other cytoplasmic proteins, which initiates signaling processes, ultimately leading to cell proliferation, differentiation, changes in metabolic activity, or cell motility (Lemmon and Schlessinger, 2010). Activated EGFR is also rapidly endocytosed (internalized) and efficiently sorted in endosomes for lysosomal degradation (Sorkin and Goh, 2009). Endocytosis and postendocytic trafficking serve as major regulators of the intensity and duration of EGFR signaling (von Zastrow and Sorkin, 2021). However, physiological mechanisms of endocytosis of EGFR and other RTKs are not well understood. As a result, experimental approaches for specifically inhibiting or accelerating EGFR endocytosis are not available. This impedes the analysis of the role of endocytosis in signaling and development of the therapeutic strategies for down-regulating EGFR and other oncogenic RTKs.

It is well established that endocytosis and endosomal sorting of EGFR and several other RTKs are regulated by their ubiquitination (reviewed in Goh and Sorkin, 2013). EGFR ubiquitination is necessary for the incorporation of receptors into intralumenal vesicles of multivesicular endosomes and their subsequent degradation in lysosomes (Eden *et al.*, 2012). Ubiquitination is also one of the two redundant mechanisms of the clathrin-mediated endocytosis (CME) of EGFR, the main physiological pathway of EGFR endocytosis (Goh *et al.*, 2010; Fortian *et al.*, 2015). EGFR ubiquitination is mediated by Casitas B-lineage lymphoma (Cbl) E3 ubiquitin ligases (Levkowitz *et al.*, 1999). In mammals, three Cbl isoforms are expressed: c-Cbl, Cbl-b, and Cbl-c. c-Cbl, generally termed as Cbl and Cbl-b, share the same domain organization. Their molecules consist of an N-terminal tyrosine kinase binding (TKB) domain, a linker region, a RING finger domain that recruits an E2 enzyme, an unfolded proline-rich region that serves for binding of SH3 domain containing proteins, and a C-terminal ubiquitin associated (UBA) domain (reviewed in Rao *et al.*, 2002; Schmidt and Dikic, 2005). The N-terminal regions (TKB-linker-RING) of all three Cbl species have high (>80%) amino acid sequence and structural homology. Cbl-c lacks most of the C-terminal sequences downstream from the RING domain and is considered not to be directly involved in RTK ubiquitination (Swaminathan and Tsygankov, 2006).

Cbl and Cbl-b are thought to be functionally redundant in regulating EGFR and to be recruited to active EGFR using the same mechanisms: direct binding of their TKB domains to the amino acid motif containing phosphorylated Y1045 (pY1045) of EGFR and indirect binding via the interaction of their proline-rich motifs with the SH3 domains of the Grb2 adaptor that binds to pY1068 and pY1086 of EGFR (Levkowitz *et al.*, 1999; Waterman *et al.*, 2002; Jiang *et al.*, 2003; Grovdal *et al.*, 2004). On the other hand, differences in phosphorylation patterns of Cbl and Cbl-b, their turnover rates in EGF-stimulated cells and an ability of their UBA domains to bind ubiquitinated proteins have been observed ([Ettenberg *et al.*, 2001; Davies *et al.*, 2004]; reviewed in [Thien and Langdon, 2005]). In some cell types, elimination of Cbl by siRNA or mouse knockout was sufficient for a robust inhibition of EGFR degradation (Duan *et al.*, 2003; Crotchett and Ceresa, 2021). However, in most cell types, efficient elimination of both Cbl and Cbl-b was necessary to achieve an inhibitory effect on EGFR ubiquitination and endocytosis, suggesting that Cbl-b can be sufficient for EGFR ubiquitination and endocytosis (for example, Mitra *et al.*, 2004; Huang *et al.*, 2006; Pennock and Wang, 2008). While numerous studies examined effects of Cbl knockdown and mouse knockout on EGFR, effects of Cbl-b knockdown and knockout on endogenous EGFR were sparsely studied (Pennock and Wang, 2008), and whether Cbl-b regulates EGFR in a manner that is fully redundant to that of Cbl is unclear. A lesser amount of information about endogenous Cbl-b could be attributed to low expression levels of Cbl-b in immortalized cell lines which had been typically used to study Cbls' function in EGFR regulation, such as HeLa, HEK293, and CHO-K1 (Baycin-Hizal *et al.*, 2012; Sigismund *et al.*, 2013; Kulak *et al.*, 2014; Cho *et al.*, 2022). Further, mechanisms of Cbls' regulation of EGFR were studied mostly in cells which do not depend on EGFR for their proliferation. Hence, we comparatively analyzed the contribution of Cbl and Cbl-b in promoting EGFR ubiquitination and endocytosis in HSC3 cell line, which is growth-dependent on EGFR (Ohnishi *et al.*, 2008; Pinilla-Macua *et al.*, 2017). Using inducible expression of wild-type (wt) or mutant recombinant Cbls and siRNA knockdowns of endogenous Cbls, we demonstrated that Cbl and Cbl-b exhibit a minimal competition for binding to EGFR and differ in the efficiency of direct versus Grb2-mediated binding to EGFR. Moreover, overexpression of dominant-negative mutants of Cbl and Cbl-b had qualitatively and quantitatively different impacts on EGF-dependent degradation of active EGFR and cell migration. Altogether, our data indicate that while both Cbl species are necessary for the most efficient EGFR ubiquitination, endocytic trafficking, and signaling, they are not mechanistically redundant in regulating these processes.

RESULTS AND DISCUSSION

Dominant-negative Cbl mutant does not block ubiquitination and endocytosis of EGFR, and Cbl-b association with the receptor

To study the role of Cbl and Cbl-b in EGFR ubiquitination and endocytosis, we began testing the effects of well-characterized RING domain mutant of Cbl (ΔC381_Cbl), that is unable to recruit E2 enzymes, on EGFR in HSC3 cells (Waterman *et al.*, 1999; Jiang and Sorkin, 2003). We anticipated that overexpression of such dominant-negative Cbl mutant will be more effective in inhibiting ligand-induced EGFR ubiquitination than an siRNA knockdown of Cbl. Overexpressed mutant was expected to block the recruitment of both endogenous Cbl and Cbl-b to EGFR, whereas Cbl-b may still bind to EGFR and compensate for Cbl function in Cbl-depleted cells. To avoid a compensatory adaptation to the constitutive overexpression, HSC3 cell line was generated that expresses the ΔC381_Cbl mutant in doxycycline (Dox)-dependent manner (Dox-on system) in a six-eight-fold excess over endogenous Cbl (Figure 1). Serum-starved cells were stimulated with 1 and 10 ng/ml EGF, physiological and supraphysiological EGF concentrations, respectively. Surprisingly, overexpression of the ΔC381_Cbl mutant only moderately decreased ubiquitination of immunoprecipitated EGFR activated with 1 or 10 ng/ml EGF (Figure 1, A and B), although weak immunoblot signals of ubiquitinated EGFR in cells stimulated with 1 ng/ml EGF were difficult to quantify as reported previously (Sigismund *et al.*, 2013; Pinilla-Macua *et al.*, 2017). This observation suggested that Cbl-b continues to catalyze EGFR ubiquitination in the presence of high amounts of the Cbl mutant. Depletion of Cbl-b by siRNA caused a moderate decrease of EGFR ubiquitination, whereas simultaneous siRNA knockdown of Cbl-b and overexpression of the ΔC381_Cbl mutant resulted in the largest decrease in

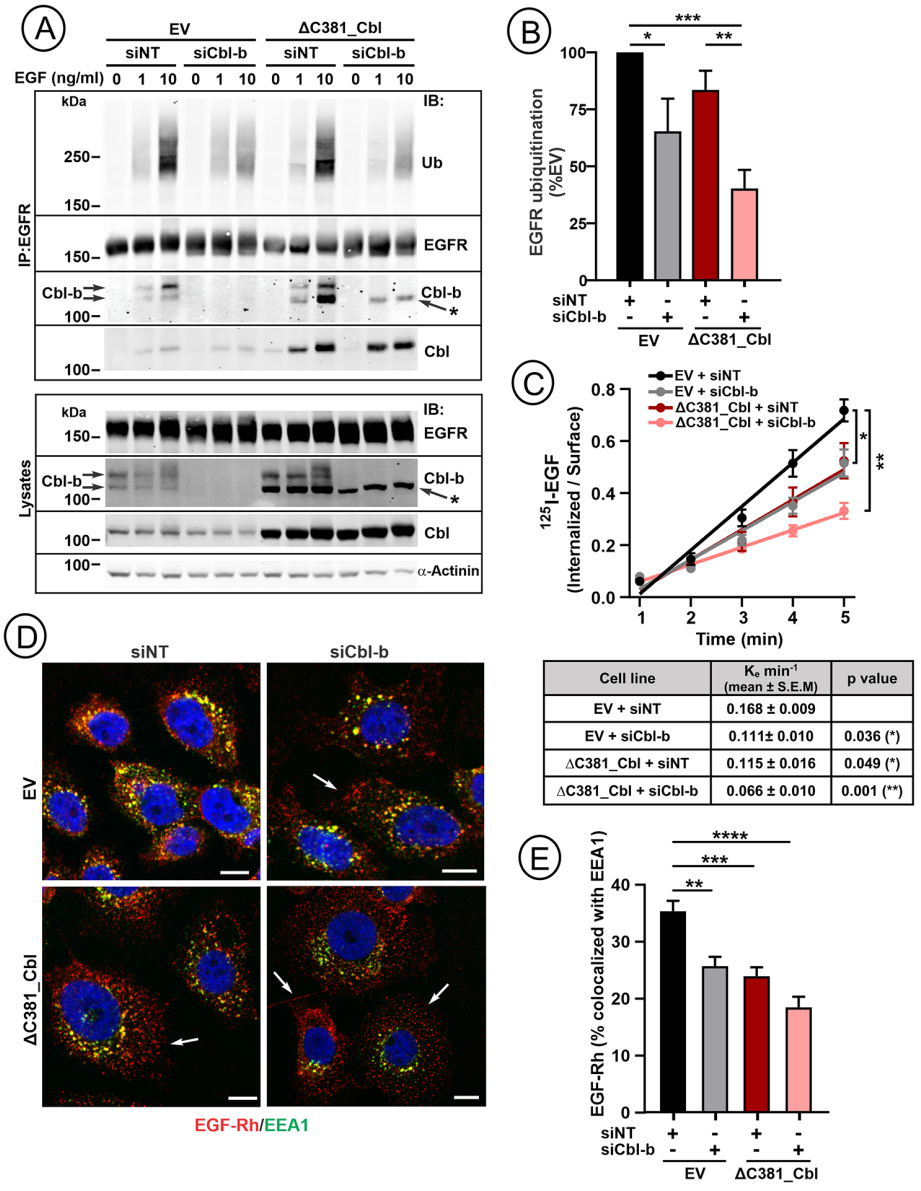

Cell line	K_e min^{-1} (mean ± S.E.M)	p value
EV + siNT	0.168 ± 0.009	
EV + siCbl-b	0.111± 0.010	0.036 (*)
ΔC381_Cbl + siNT	0.115 ± 0.016	0.049 (*)
ΔC381_Cbl + siCbl-b	0.066 ± 0.010	0.001 (**)

FIGURE 1: Overexpression of the Cbl mutant lacking E3 ligase activity does not substantially inhibit ligand-induced ubiquitination and endocytosis of EGFR in HSC3 cells. HSC3 Dox-on cells expressing empty vector (EV) or ΔC381_Cbl mutant were transfected with nontargeting (siNT) or Cbl-b siRNA (siCbl-b). Cells were untreated or stimulated with 1 or 10 ng/ml EGF for 15 min at 37°C, lysed, and EGFR was immunoprecipitated. Immunoprecipitates and aliquots of lysates were resolved by SDS–PAGE and probed by western blotting with antibodies to ubiquitin (Ub), EGFR, Cbl, Cbl-b, and α-actinin (loading control). (A) Western blot of the representative experiment is shown. Arrows point to two species of endogenous Cbl-b which presumably correspond to two variants of Cbl-b (NCBI sequences: NM_001321786.1 and NM_001321793.2). Recombinant Cbl-b corresponds to the smaller species of ~125 KDa. Note that a batch of Cbl-b antibodies used in this experiment cross-reacted with overexpressed ΔC381_Cbl mutant (asterisk). (B) Quantification of the effects of Cbl mutant and siCbl-b on EGFR ubiquitination in cells stimulated with 10 ng/ml EGF from experiments exemplified in (A). Bar graph represents mean values of the ratio of ubiquitinated EGFR to total EGFR expressed as percent of this ratio in EV cells transfected with siNT and treated with 10 ng/ml EGF (±SEM, $n = 9$–11). One-way ANOVA tests were performed. p values are against "EV+siNT." *$p < 0.0332$, **$p < 0.0067$, ****$p < 0.0001$. (C) Internalization of ^{125}I-EGF in EV and ΔC381_Cbl expressing cells transfected with siNT or siCbl-b. The mean ratio of internalized/surface ^{125}I-EGF at each timepoint (±SEM; $n = 3$) is plotted against time. K_e values were calculated using linear regression slopes exemplified in the graph. Table summarizes K_e values (±SEM; $n = 3$). One-way ANOVA tests were performed. p values are against "EV+siNT." *$p < 0.0332$, **$p < 0.0021$. (D) Cells were incubated with 4 ng/ml EGF-Rh for 10 min at 37°C, fixed, permeabilized, and labeled with EEA1 antibodies. Imaging was through the 640-nm (*green*, EEA1), 561-nm (*red*, EGF-Rh), and 405-nm (*blue*, nuclei) channels. Merged-channel, maximum intensity projection images of the same two confocal planes from z-stacks are presented. Fluorescence intensity scales are identical for all images. White arrows mark examples of peripheral small puncta of EGF-Rh which are not colocalized with EEA1. Scale bars, 10 μm. (E) Quantifications of the fraction of EGF-Rh colocalized with EEA1 of total cell-associated EGF-Rh fluorescence in images exemplified in (D). Bar graph represents mean values of the percent of EGF-Rh colocalized with EEA1 (±SEM, n = 6–7 FOVs). One-way ANOVA tests were performed. p values are against "EV+siNT." **$p = 0.0031$; ***$p = 0.008$; ****$p < 0.0001$.

EGFR ubiquitination. Endogenous Cbls and recombinant Cbl mutant were efficiently immunoprecipitated with EGFR activated with 1 or 10 ng/ml. Importantly, an excess of the ΔC381_Cbl mutant did not appear to affect Cbl-b coimmunoprecipitation with EGFR stimulated with either 1 or 10 ng/ml EGF (Figure 1A).

Similar trends were observed in the effects of ΔC381_Cbl and Cbl-b siRNA on EGFR internalization rates measured using 1 ng/ml ^{125}I-EGF, a concentration favoring CME of EGFR (Figure 1C). While both ΔC381_Cbl mutant and Cbl-b siRNA moderately decreased the internalization rate constant K_e, the combined effect was significantly stronger (Figure 1C). Endocytosis-inhibitory effects of the ΔC381_Cbl mutant and Cbl-b siRNA alone or in combination were also observed by fluorescence microscopy imaging of cells stimulated with the EGF-Rhodamine conjugate (EGF-Rh; 4 ng/ml). These effects were manifested by a reduced fraction of EGF-Rh detected in large perinuclear puncta colocalized with the early/sorting endosome marker EEA1, and an increased number of small puncta located at cell periphery and edges (Figure 1, D and E). In both types of assays, maximal inactivation of Cbls resulted in a partial inhibition of EGFR internalization via CME due to compensation by other Cbl-independent mechanisms of EGFR CME, and possibly, clathrin-independent endocytosis (in experiments where 4 ng/ml EGF-Rh was used; Goh *et al.*, 2010). Altogether, the data in Figure 1 imply that two Cbl species functionally compensate for each other by acting independently in promoting EGFR ubiquitination and endocytosis, and that there might be quantitatively or qualitatively different mechanisms of EGFR interaction with Cbl and Cbl-b.

To comparatively analyze observations in HSC3 cells presented in Figure 1 in another

oral squamous cell carcinoma cells, we generated clonal variants of OSC-19 cells (Yokoi *et al.*, 1988) expressing EV or the ΔC381_Cbl mutant in a Dox-dependent manner. OSC-19 cells display growth sensitivity to gefitinib indicative of their growth-dependence on the EGFR activity (Xu *et al.*, 2011). However, OSC-19 cells express Cbl-b at a much lower level compared with HSC3 cells (Supplemental Figure S1). Nevertheless, overexpression of ΔC381_Cbl mutant did not eliminate EGF-induced coimmunoprecipitation of endogenous Cbl-b with EGFR and EGFR ubiquitination in OSC-19 cells (Supplemental Figure S2A). Furthermore, combination of ΔC381_Cbl–mutant overexpression and siRNA depletion of Cbl-b was necessary for the strongest inhibition of EGF-Rh endocytosis which was measured by the analysis of EGF-Rh colocalization with EEA1 (Supplemental Figure S2, B and C). Given the similarity of the results in HSC3 and OCS-19 cells presented in Figures 1 and Supplementary Figure S2, but a much higher expression of Cbl-b in HSC3 cells, we performed the subsequent experimental analysis aimed at elucidating differences between Cbl and Cbl-b activities in HSC3 cells.

The ability of Cbl and Cbl-b to functionally compensate for each other is not unexpected. In fact, depletion of both proteins was necessary to robustly inhibit EGFR ubiquitination and endocytosis in most experimental models previously studied (for example, Sigismund *et al.*, 2013; Fortian *et al.*, 2015). The inability of the ΔC381_Cbl mutant to significantly inhibit EGFR ubiquitination and endocytosis, which implied the existence of different mechanisms of Cbl and Cbl-b binding to EGFR, was unforeseen. To our knowledge, all studies using overexpression of similar E3-ligase activity-deficient Cbl mutants reported strong inhibition of EGFR ubiquitination and degradation (for example, Waterman *et al.*, 1999). However, many previous studies were performed in cells, such as HeLa, with the substantially lower Cbl-b expression level than in HSC3 cells (for example, Jiang and Sorkin, 2003; Sigismund *et al.*, 2013; Supplemental Figure S1). Furthermore, early studies of Cbl and Cbl-b were often performed in cells overexpressing recombinant Cbls and/or EGFR, and/or used very high EGF concentrations, which mistargets EGFR to nonphysiological trafficking pathways.

Overexpression of Cbl, Cbl-b, and their mutants does not block binding of a counterpart Cbl species to EGFR

To quantitatively analyze the crosstalk between Cbl and Cbl-b during their recruitment to ligand-activated EGFR, HSC3 cell lines were generated that overexpress wt Cbl-b (wtCbl-b) or RING domain mutant of Cbl-b (C373A_Cbl-b; Ettenberg *et al.*, 2001; Peschard *et al.*, 2007) in Dox-on dependent manner. HSC3 cells inducibly expressing wt Cbl (wtCbl) were generated in our previous studies (Pinilla-Macua *et al.*, 2017). To express various Cbl/Cbl-b variants at a comparable level, the cells were induced with Dox in the presence of different concentrations of sodium butyrate which potentiates the activity of the CMV promoter (de Poorter *et al.*, 2007). EGFR was immunoprecipitated in serum-starved or EGF-stimulated cells expressing wt or mutant Cbls, and the amount of Cbls was quantitated in these immunoprecipitates. Overexpression of wtCbl-b and C373A_Cbl-b (~7- and ~4.5-fold, respectively; Figure 2, A and B; Supplemental Figure S3A) led to a reduced coimmunoprecipitation of endogenous Cbl with EGFR, although a significant amount of Cbl was still present in immunoprecipitates (Figure 2, A and C). By contrast, excess of wtCbl or ΔC381_Cbl (~3- and ~5-fold, respectively; Figure 2B; Supplemental Figure S3A) did not significantly decrease Cbl-b association with EGFR (Figure 2, A and C). It should be noted that endogenous Cbl-b expression was found to be slightly higher in the presence of ΔC381_Cbl mutant than in EV cells in some experiments (for example, Figure 1A), but this trend was not statistically significant (Figure 2B). Our observation of the ability of Cbl-b to displace a fraction of endogenous Cbl from EGFR agrees with the previous demonstration of such displacement of overexpressed recombinant Cbl by cooverexpressed Cbl-b in HEK293 cells also overexpressing recombinant EGFR (Ettenberg *et al.*, 1999).

The data in Figure 2, A–C must be considered in the context of intracellular concentrations of endogenous and recombinant Cbl and Cbl-b. Supplemental Figure S1 shows that the amount of Cbl in HSC3 cells is similar to that in HeLa cells where it is estimated to be ~30,000 copies per cell (Kulak *et al.*, 2014). Therefore, ~3–5-fold overexpression results in ~90,000–150,000 recombinant Cbl molecules per cell. Endogenous Cbl-b level is ~5-fold higher in HSC3 than in HeLa cells (Supplemental Figure S2) where it is estimated to be < 2000 copies per cell (Kulak *et al.*, 2014). Therefore, with ~10,000 endogenous Cbl-b molecules/HSC3 cell, 4.5–7-fold overexpression of Cbl-b in our experiments resulted in ~45,000–70,000 molecules of recombinant Cbl-b per cell. Thus, overexpressed Cbl-b was not at a high molar excess to endogenous Cbl in Figure 2 experiments, yet Cbl-b competed out a fraction of Cbl from EGFR. In contrast, overexpressed Cbl and its mutant were at least in a nine-fold molar excess over endogenous Cbl-b, albeit with no effect on Cbl-b coimmunoprecipitation with EGFR. These observations together with the data in Figure 1A (Cbl-b immunoprecipitation in the presence of a large excess of the Cbl mutant) indicate that Cbl-b interaction with EGFR is either stronger than that of Cbl, or Cbl-b has an additional mode of the interaction with EGFR which is unavailable to Cbl. In fact, Cbl-b but not Cbl was proposed to bind mutant EGFR truncated at residue 1044, suggesting the possibility of Cbl-b: EGFR association independent of pY1045 and Grb2, although the mechanism of such interaction is unknown (Pennock and Wang, 2008).

Together, the data of Figure 2, A–C show that both Cbl and Cbl-b are capable of the recruitment to activated EGFR through nonredundant or partially redundant mechanisms. One possible mode of Cbl or Cbl-b binding to EGFR in the presence of an excess of a counterpart species could be via their heterodimerization. The UBA domains of Cbl and Cbl-b were proposed to mediate their homo- and heterodimerization (Kozlov *et al.*, 2007; Peschard *et al.*, 2007). Therefore, we tested whether inducible expression of the Cbl-b mutant lacking the UBA domain (ΔUBA_Cbl-b) affects Cbl coimmunoprecipitation with EGFR. As shown in Figure 2, A and C, the ΔUBA_Cbl-b mutant partially displaced Cbl from EGFR to the same extent as did wtCbl-b and the C373A_Cbl-b mutant (Figure 2, A–B), indicating that heterodimerization is not responsible for the residual coimmunoprecipitation of Cbl with EGFR. Because the UBA domain of Cbl-b was shown to efficiently interact with ubiquitinated proteins (Davies *et al.*, 2004), these data also show that such interactions are not involved in Cbl-b binding to EGFR.

As expected, overexpression of the RING mutants of Cbl and Cbl-b only partially reduced EGFR ubiquitination (Figure 2D), likely because a substantial amount of endogenous Cbl or Cbl-b remained associated with the receptor. To assess whether Cbl association with EGFR and EGFR ubiquitination (both measured using 10 ng/ml EGF) correlate with EGF-induced EGFR internalization, ^{125}I-EGF internalization rates (1 ng/ml was used to measure rates of CME) were measured in each HSC3 cell clone grown without or with Dox to induce wt or mutant Cbls' expression. As shown in Figure 2E, mutant overexpression that partially decreased EGFR ubiquitination correlated with low K_e values. Increased EGFR ubiquitination in cells overexpressing wtCbl-b (by ~25%), however, did not lead to a higher internalization rate, presumably, because of the limited capacity of the EGFR CME pathway (Sorkin and Goh, 2009).

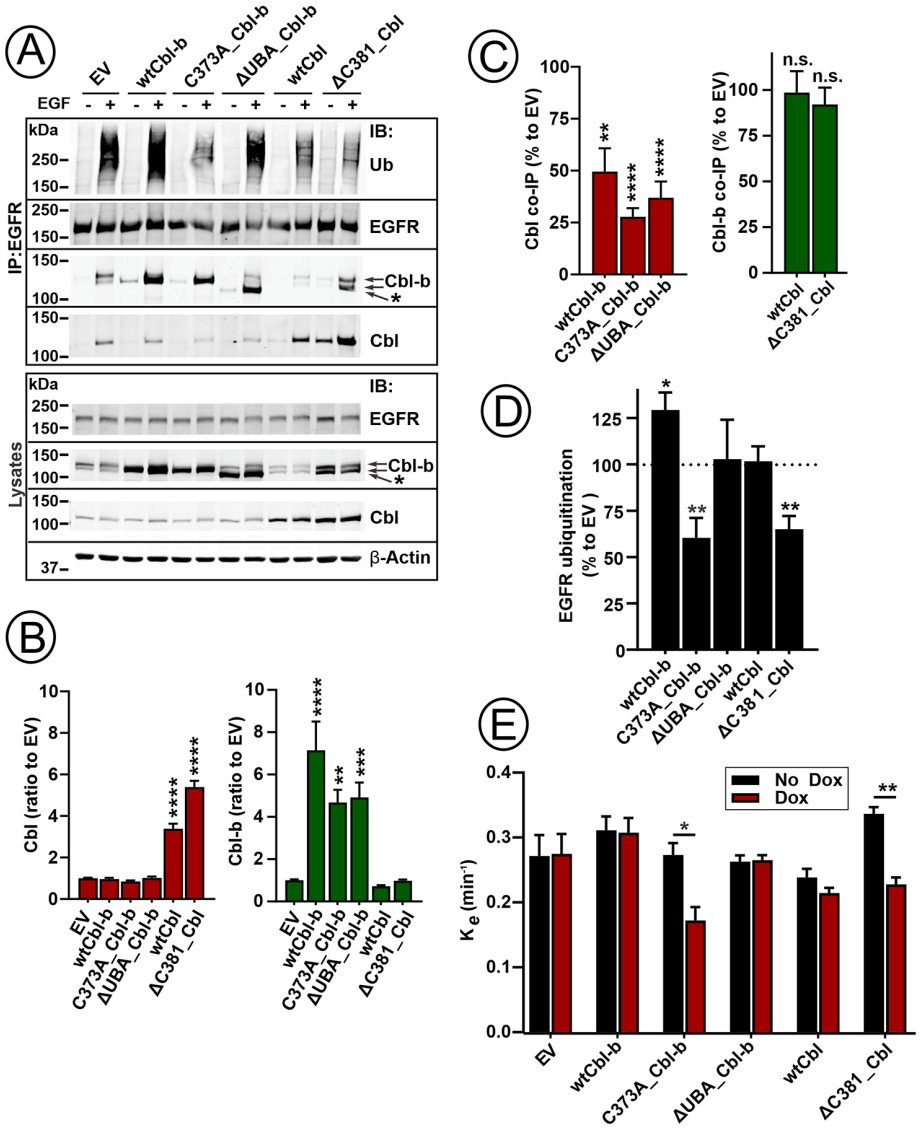

FIGURE 2: Endogenous Cbl and Cbl-b are recruited to EGFR and regulate EGFR in the presence of overexpressed dominant-negative mutants of homologues species. (A–C) HSC3 Dox-on cells expressing wt or mutant Cbl or Cbl-b were incubated with or without 10 ng/ml EGF for 15 min, lysed, and EGFR was immunoprecipitated. Immunoprecipitates were probed by western blotting with EGFR, ubiquitin (Ub), Cbl, and Cbl-b antibodies. Aliquots of lysates were probed by western blotting with EGFR, Cbl, Cbl-b, and β-Actin antibodies (loading control). (A) Representative western blot of immunoprecipitates and lysates. Arrows point out two species of endogenous Cbl-b. Recombinant Cbl-b corresponds to a smaller species of ~125 KDa. Note that a batch of Cbl-b antibodies used in this experiment weakly recognizes Cbl which is evident on the lanes corresponding to overexpressed ΔC381_Cbl mutant (asterisk). (B) Bar graphs summarize quantification of Cbl and Cbl-b expression levels in lysates normalized to β-actin. Mean values of the amount of Cbl-b (green) and Cbl (red) ratio to those amounts in EV cells are presented (±SEM, $n = 16–18$). One-way ANOVA was performed. p values are against "EV." $^{**}p < 0.0041$, $^{***}p < 0.0004$, $^{****}p < 0.0001$. (C) Quantification of endogenous Cbl and Cbl-b coimmunoprecipitation with EGFR in EGF-treated cells in experiments exemplified in (A). Bar graphs represent mean values (±SEM, $n = 7–9$) of Cbls' coimmunoprecipitation with EGFR corrected for each protein expression level measured in total cell lysates and calculated as percent of coimmunoprecipitated Cbl/Cbl-b in EGF-treated EV cells. Unpaired t tests were performed. p values are against "EV+EGF." ns, not significant, $^{**}p < 0.0021$, $^{****}p < 0.0001$. Quantification of the amounts of Cbl-b in IPs and lysates were limited to the 130-kDa species. (D) Quantification of EGFR ubiquitination in EGF-treated cells in experiments exemplified in (A). The amount of ubiquitin immunoreactivity in EGFR immunoprecipitates was normalized for total immunoprecipitated EGFR and expressed as percent to this normalized amount in EGF-treated EV cells. Bar graph represents mean values (±SEM, $n = 9$). Unpaired t tests against "EV+EGF" were performed. ($^{*}p < 0.0332$, $^{**}p < 0.0021$). (E) HSC3 Dox-on cells expressing wt or mutant Cbl or Cbl-b were grown without or with Dox to induce Cbls expression. The ^{125}I-EGF internalization rate constant K_e was measured as in Figure 1C. The bar graph depicts mean values of K_e (±SEM, $n = 5$) measured in cells induced (DOX) and not induced (No Dox) to express Cbls. One-way ANOVA tests were performed. p values are against "EV." $^{*}p < 0.0182$, $^{**}p < 0.0043$.

Coimmunoprecipitation of EGFR and Cbls may depend on the sensitivity of their interactions to detergents and other components in the lysis buffer. Therefore, we utilized an additional approach in which the ratio of the amounts of Cbls and labeled EGF colocalized in endosomes is quantified as a surrogate measure of Cbls' association with active EGFR (Jiang and Sorkin, 2003; Perez Verdaguer *et al*., 2021). This approach was feasible because: i) some extent of ligand-induced EGFR endocytosis was observed in all overexpression settings (Figures 1, D and E and 2E); and ii) Cbls are translocated to endosomes only if bound to EGF-activated EGFR. In cells not treated with EGF, all endogenous and overexpressed Cbl proteins and their mutants detected by immunofluorescence labeling were distributed throughout the cytoplasm (Supplemental Figure S4A). Stimulation of cells with 4 ng/ml EGF-A647 for 15 min resulted in the accumulation of all variants of Cbl proteins in endosomes containing EGF-A647 (Figure 3, A and B) which is consistent with only a partial (20–30%) inhibition of EGF-Rh endocytosis observed in Figure 1, D–E. Importantly, endogenous Cbl and Cbl-b were detected in EGF-A647 positive endosomes despite overexpression of wt or mutant counterpart species. Moreover, overexpression of wt or mutant Cbls did not significantly affect the ratio of endogenous Cbl or Cbl-b to EGF-A647 in endosomes, except that ΔUBA_Cbl-b reduced the Cbl/EGF-A647 ratio, indicative of a partial displacement of Cbl from EGF-A647:EGFR complexes by this mutant (Figure 3C). The effects of recombinant Cbl-b expression on Cbl colocalization (association) with EGFR in this assay were less pronounced as compared with what was observed in the coimmunoprecipitation assay (Figure 2C). Such difference is expected because the colocalization assay quantifies only internalized EGF-A647:EGFR complexes that are colocalized with Cbls whereas those complexes that are not colocalized with Cbls, as well as plasma membrane EGFRs are not accounted for. Nevertheless, Figure 3 confirms that overexpression of Cbls does not significantly

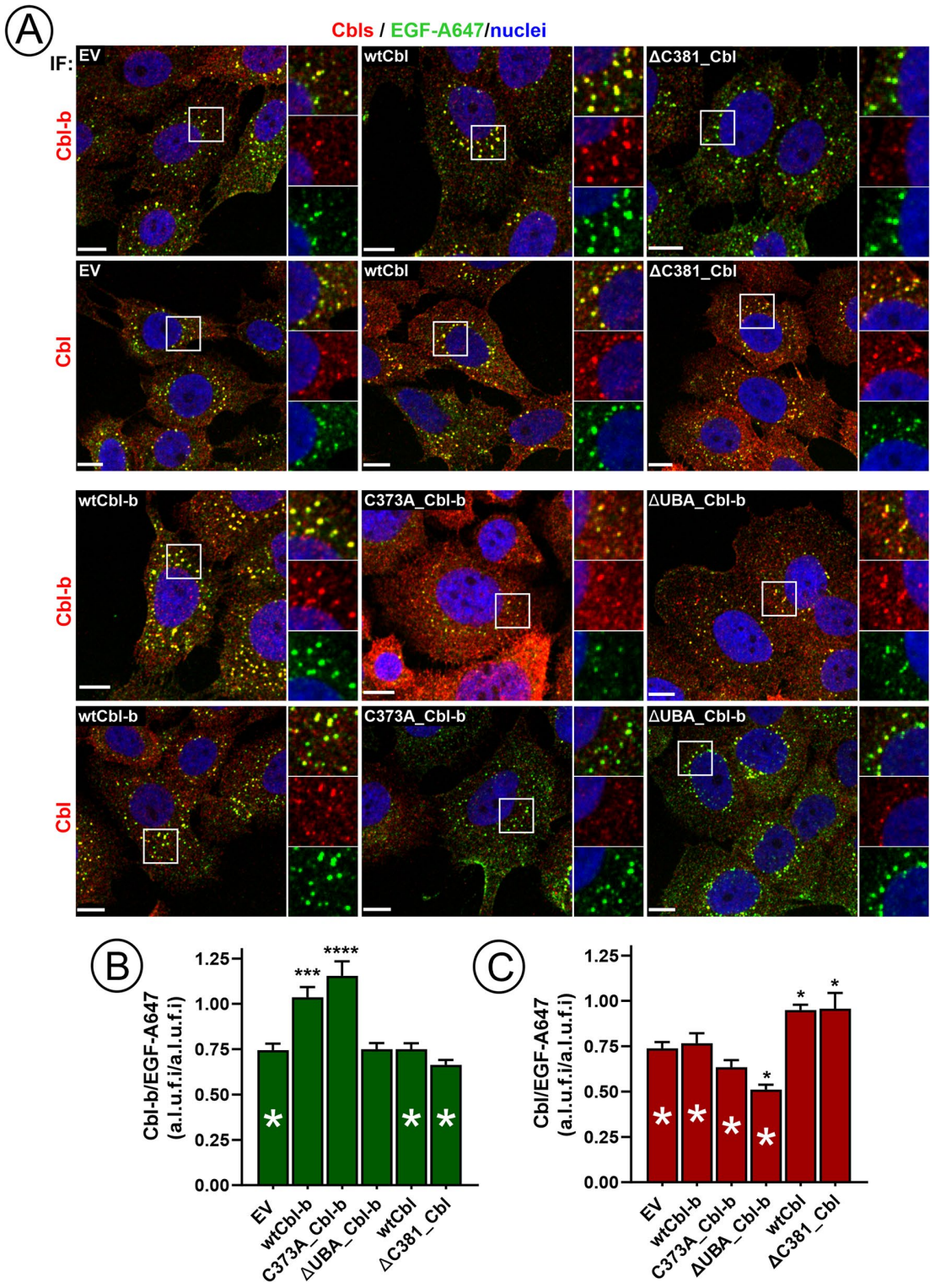

FIGURE 3: Effects of Cbl/Cbl-b mutant overexpression on colocalization of Cbl and Cbl-b with endosomal EGF:EGFR complexes. HSC3 Dox-on cells expressing EV, wt, or mutant Cbl or Cbl-b (indicated in white letters) were treated with 4 ng/ml EGF-Alexa647 for 15 min at 37°C, fixed, permeabilized, and stained (IF) with antibodies for Cbl or Cbl-b. Three-dimensional imaging was performed through 405-nm (*blue*, nuclei), 561-nm (*red*, Cbls), and 640-nm (*green*, EGF-A647) channels. (A) Representative single-plane merged images of Cbl-b or Cbl immunofluorescence and EGF-A647 fluorescence. Insets are high magnification images of individual and merged fluorescence channels of the regions indicated by white rectangles. Scale bars, 10 μm. (B and C) Quantification of the ratio of arbitrary linear units of fluorescence intensity (a.l.u.f.i.) of Cbl or Cbl-b to that of EGF-A647 fluorescence in endosomes from images exemplified in (A). Bar graphs represent mean value of Cbl-b/EGF-A647 (B) and Cbl/EGF-A647 ratios (C; ±SEM; $n = 10$). White asterisks indicate quantifications of endogenous Cbl-b or Cbl. p values were calculated using one-way ANOVA. p values are against "EV." *$p < 0.0332$, ***$p < 0.0021$, ****$p < 0.0001$.

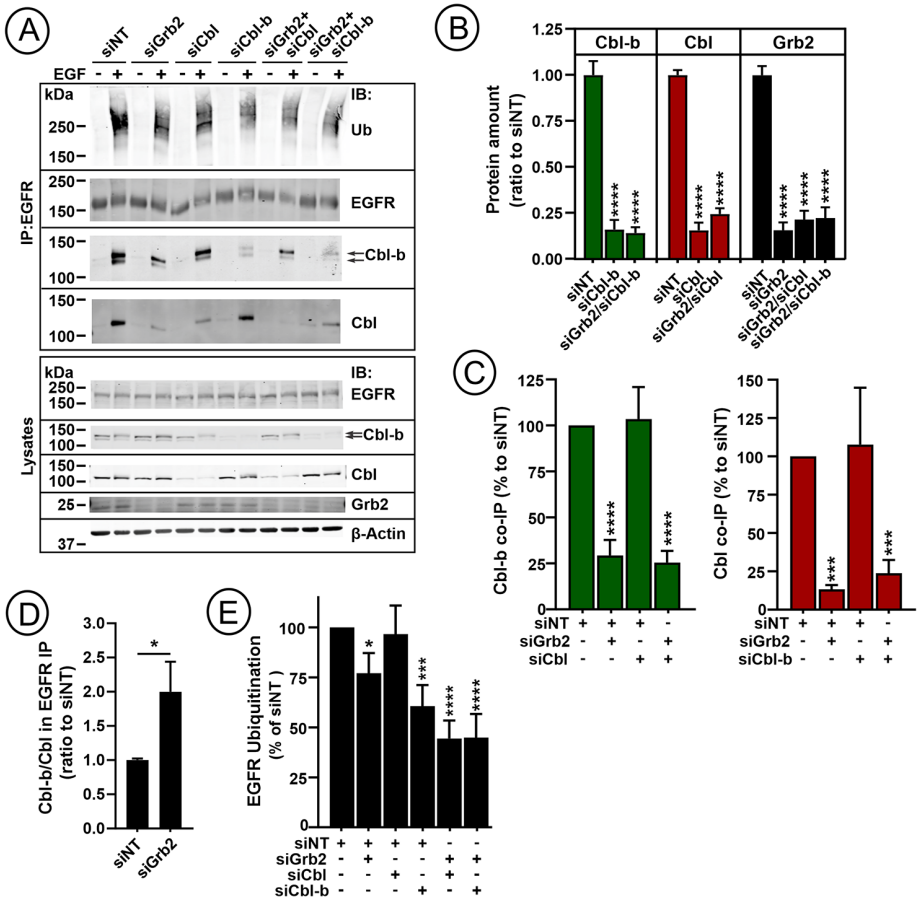

FIGURE 4: Grb2 contributes to EGFR binding of Cbl to a larger extent than to the receptor binding of Cbl-b. Parental HSC3 were transfected with siRNA duplexes targeting Grb2, Cbl and/or Cbl-b as indicated. The cells were stimulated with 10 ng/ml EGF for 15 min. EGFR was immunoprecipitated, and immunoprecipitates were probed by western blotting with EGFR, ubiquitin (Ub), Cbl, and Cbl-b antibodies. Cell lysates were probed with antibodies to EGFR, Cbl, Cbl-b, Grb2, and β-Actin (loading control). (A) Representative western blots of immunoprecipitates and lysates. Arrows point out two species of endogenous Cbl-b. (B) Quantification of the efficiencies of Cbl-b, Cbl, and Grb2 knockdowns. The bar graph shows mean values of the ratio of the amounts of proteins in siRNA-transfected cells to the amount of the same protein in siNT-transfected cells (±SEM, $n = 8–16$). One-way ANOVA to siNT cells was performed. p values are against "siNT" cells. ****$p < 0.0001$. (C) Quantification of Cbl coimmunoprecipitation with EGFR in EGF-treated cells in experiments exemplified in (A). Bar graphs represent mean values of Cbls coimmunoprecipitated as percent to siNT cells (±SEM, $n = 5–11$). One-way ANOVA was performed. p values are against "siNT" cells. ***$p < 0.0002$, ****$p < 0.0001$. (D) Ratio of coimmunoprecipitated Cbl-b/Cbl immunoreactivity in cells transfected with siGrb2 was normalized to this ratio in siNT cells (mean ±SEM, $n = 6$). Unpaired t test was used. *$p < 0.0332$. (E) Quantification of EGFR ubiquitination in EGF-treated cells in experiments exemplified in (A). Bar graph represents mean values of EGFR ubiquitination, measured as ratio Ub-EGFR/total EGFR (±SEM, $n = 6–11$) and expressed as percent of the ratio in siNT cells. Unpaired t tests were performed against "siNT" cells. *$p < 0.0332$, ***$p < 0.0002$, ****$p < 0.0001$.

compete out their counterpart species from EGFR. Therefore, data in Figure 3 are consistent with findings in Figure 2 in supporting the hypothesis of distinct or partially redundant mechanisms of Cbl and Cbl-b interactions with EGFR.

Different dependency of Cbl and Cbl-b recruitment to EGFR on pY1045 and Grb2

To compare the efficiency of two modes of Cbl and Cbl-b interaction with EGFR, direct binding to pY1045 and indirect binding via Grb2, and their importance for EGFR ubiquitination, we first examined the role of Grb2 in Cbls' coimmunoprecipitation with EGFR. To this end, Grb2 was depleted using well-characterized siRNA duplex (Jiang *et al.*, 2003) alone or together with siRNA depletion of Cbl or Cbl-b (Figure 4, A–B). As shown in Figure 4, A–C, Grb2 knockdown reduced coimmunoprecipitation of both Cbl and Cbl-b with EGFR. However, this decrease was significantly more pronounced for Cbl than for Cbl-b because the fraction of Cbl-b remaining in EGFR immunoprecipitates in Grb2-depleted cells relative to that fraction of Cbl-b in EGFR immunoprecipitates from control cells was ~2-fold larger than such fraction of Cbl (Figure 4, C–D). This observation indicates that Cbl binding to ligand-activated EGFR depends on Grb2 to a significantly greater extent than Cbl-b binding. Individual knockdown of Cbls did not affect coimmunoprecipitation of the other isoform with EGFR (Figure 4C), further arguing against the role of Cbls' heterodimerization in their interaction with EGFR. Depletion of Grb2 or Cbl-b but not of Cbl partially decreased EGFR ubiquitination, whereas the strongest reduction of EGFR ubiquitination was caused by the combination of Grb2 siRNA with the knockdown of either Cbl protein (Figure 4E). The data in Figure 4 suggest that both Grb2-dependent and -independent binding modes of Cbls to EGFR are necessary for the most efficient EGFR ubiquitination and further demonstrate that Cbl and Cbl-b functionally compensate for each other. These data also imply that Cbl-b may be a more efficient EGFR E3 ligase than Cbl: while Cbl-b depletion was not fully compensated for by Cbl despite a higher intracellular concentration of the latter, Cbl-b fully compensated for siRNA-depleted Cbl. This hypothesis agrees with the observation of an apparently stronger association with EGFR of Cbl-b than Cbl (Figure 2).

Analysis of EGFR immunoprecipitation experiments exemplified in Figures 1, 2, and 4 suggest that under conditions of our experiments (a fraction of total cellular EGFRs is activated for 15 min; Supplemental Figure S5), EGFR ubiquitination is not linearly proportional to the amount of Cbls associated with EGFR measured by coimmunoprecipitation. For example, a maximal level of EGFR ubiquitination was achieved in Cbl-depleted cells despite that the extent of Cbl-b coimmunoprecipitation with EGFR did not increase (compared with that in control cells) to compensate for the lack of Cbl (Figure 4, C and E). In fact, a sigmoid-like relationship between EGFR activity (tyrosine phosphorylation) and ubiquitination was demonstrated in HeLa and NR6 cells where EGFR ubiquitination plateaued at EGF concentrations of ~10 ng/ml (Sigismund *et al.*, 2013; Pinilla-Macua *et al.*, 2017). Finally,

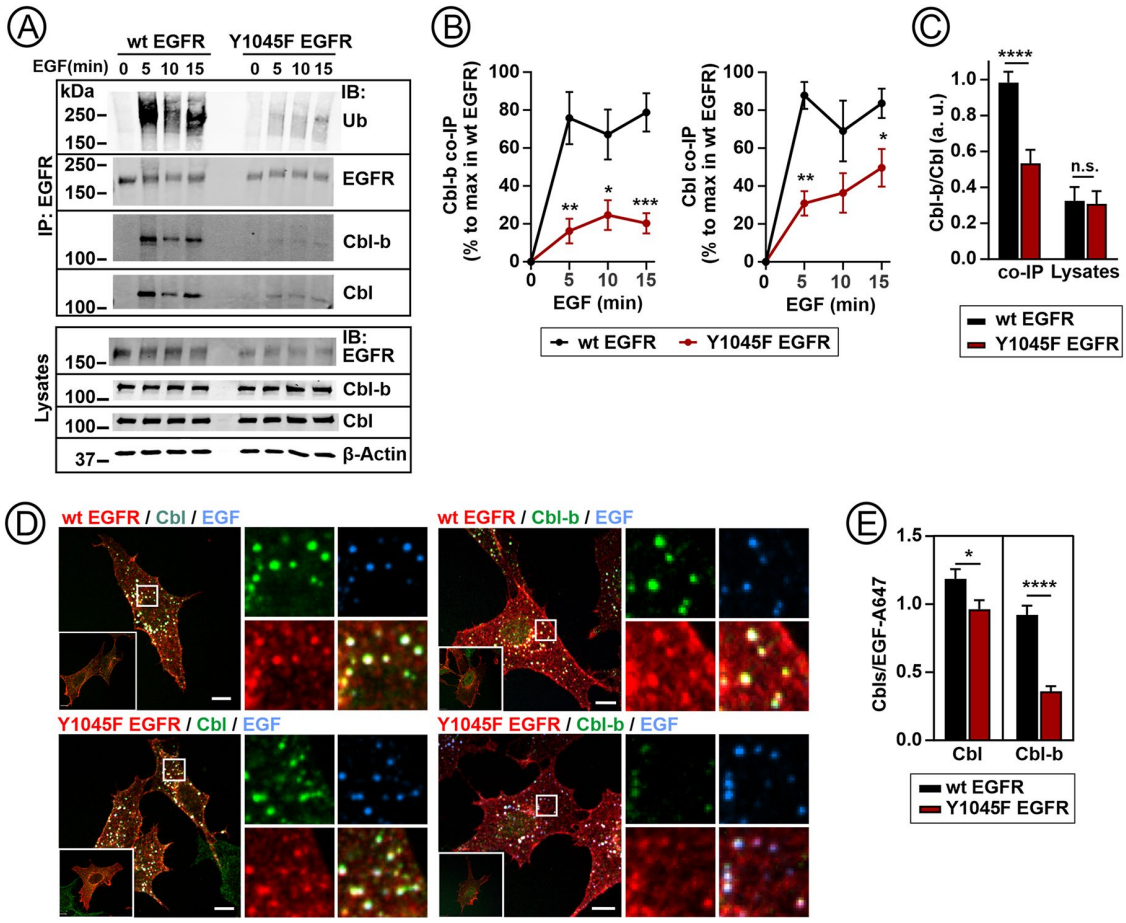

FIGURE 5: Cbl-b depends on pY1045 for binding to EGFR to a larger extent than does Cbl. (A–C) PAE cells expressing wt EGFR or the Y1045F EGFR mutant were incubated with 10 ng/ml EGF for 0–15 min at 37°C. EGFR was immunoprecipitated. The immunoprecipitates and lysates were probed with ubiquitin (Ub), EGFR, Cbl, Cbl-b, and β-Actin (loading control) antibodies. (A) Representative western blots. (B) Quantification of experiments exemplified in (A). The amounts of immunoprecipitated Cbls normalized to the amount of immunoprecipitated EGFR are expressed as percent of the maximum coimmunoprecipitated Cbl or Cbl-b measured in wt EGFR cells in each experiment. Mean values are plotted against time (±SEM, $n = 6$). Unpaired t test was used for each time point (Y1045F against wt EGFR). *$p < 0.0332$, **$p < 0.0021$, ***$p < 0.0002$. (C) Quantification of the ratio of Cbl-b and Cbl immunoreactivities in EGFR immunoprecipitates (co-IP) and cell lysates in experiments exemplified in (A). Bar graph represents mean ratio values in cells treated with EGF (±SEM; $n = 6$). Unpaired t test was performed. ns. nonsignificant, ****$p < 0.0001$. (D–E) PAE cells expressing wt or Y1045F EGFR mutant were incubated with 4 ng/ml EGF-A647 for 15 min at 37°C, fixed, permeabilized, and stained with antibodies to EGFR and Cbl or Cbl-b. Three-dimensional imaging was performed through 488-nm (*green*, Cbl or Cbl-b), 561-nm (*red*, EGFR), and 640-nm (*cyan*, EGF-A647) channels. (D) Representative confocal images with merged channels are shown. Insets depict untreated cells (left bottom) and high magnification images (separated channels and the merge) of the regions marked by the white square (on the right). Scale bars, 10 μm. (E) Quantification of the ratio of fluorescence intensities (a.l.u.f.i.) of Cbl and Cbl-b to EGF-A647 in endosomes. Bar graph represents mean values (±SEM, $n = 16–20$ cells). Unpaired t test was performed. *$p < 0.0332$, ****$p < 0.0001$.

the possibility that other E3 ligases may compensate for the depletion of Grb2, Cbl, and/or Cbl-b cannot be ruled out, given that the inhibition of EGFR ubiquitination in HSC3 and OSC-19 cells was not complete under any conditions (Figures 1, 2, and 4; Supplemental Figure S2).

To examine the contribution of the direct binding of Cbls to pY1045 of EGFR, we used porcine aortic endothelial (PAE) stable cell lines expressing human wtEGFR or the Y1045F EGFR mutant, described in our previous studies (Jiang and Sorkin, 2003). PAE cells do not express endogenous EGFR or other ErbBs, and thus, represent a useful model to study effects of EGFR mutations. As shown previously, the Y1045F mutation dramatically decreased EGFR ubiquitination (Levkowitz *et al.*, 1999; Jiang and Sorkin, 2003; Figure 5A). Coimmunoprecipitation of Cbl and Cbl-b with the Y1045F mutant was also reduced as compared with their coimmunoprecipitation with wtEGFR (Figure 5, A and B). However, this reduction was significantly more pronounced in the case of Cbl-b than Cbl, especially at 15 min of EGF stimulation (Figure 5, A and B). Quantification of the ratio of the amounts of Cbl-b and Cbl revealed relative enrichment of Cbl over Cbl-b in the immunoprecipitates of the Y1045F mutant (Figure 5C). This observation indicates that while binding of both Cbls to EGFR is in part mediated by the pY1045-contaning motif, this interaction mechanism is more important for Cbl-b than Cbl.

The Y1045F mutation does not affect the rate of EGFR internalization via CME (Jiang and Sorkin, 2003), which allowed us to

employ the "endosome colocalization" approach to additionally analyze Cbls' recruitment to the Y1045F mutant versus wtEGFR. Immunofluorescence labeling of Cbls in PAE cells stimulated with EGF-A647 demonstrated that endogenous Cbl and Cbl-b are colocalized with EGF-A647 in endosomes in both cell lines expressing wt or mutant EGFR (Figure 5D). However, the stoichiometry of Cbl and Cbl-b to EGF-A647 in endosomes was lower in mutant-expressing cells than in wtEGFR-expressing cells (Figure 5E). Importantly, Cbl-b/EGF-A647 ratio was significantly lower than the Cbl/EGF-647 ratio in Y1045F expressing cells (Figure 5E). These data together with the immunoprecipitation experiments with PAE and HSC3 cells (Figures 4 and 5, A–C) prompted us to propose a model whereby Grb2- and pY1045-mediated interaction modes contribute to the recruitment of Cbl and Cbl-b to activated EGFR at a different extent; the former is more significant for Cbl:EGFR interaction and the latter is predominant for Cbl-b:EGFR interaction.

High-resolution structures of the TKB domains of Cbl and Cbl-b are nearly identical (for example, Protein Data Bank [PDB] codes: 3PFV, 3VGO, and 3ZNI; see also Ohno *et al*., 2016) and do not provide clues to explain the different efficiency and/or strength of Cbl and Cbl-b interactions with the pY1045 motif observed in our experiments. Interestingly, only Cbl-b, but not Cbl, binds directly to phosphotyrosine motifs of another RTK, platelet-derived growth factor receptor β (PDGFR β; Rorsman *et al*., 2016). Likewise, to our knowledge, there is no experimental data that would explain a stronger contribution of Grb2-mediated interaction with EGFR of Cbl compared with that of Cbl-b. In our experiments, the amounts of activated EGFR and Grb2 are not limiting factors because overexpression of Cbl or Cbl-b resulted in their increased coimmunoprecipitation and colocalization with EGFR (Figures 1–3). Based on estimated intracellular concentrations of Cbl and Cbl-b, the number of Grb2:Cbl complexes, which preexist in unstimulated cells, is predicted to be three times larger than this number of Grb2:Cbl-b complexes in HSC3 cells, which may explain a greater role of this interaction mode in Cbl function on EGFR. In agreement, siRNA knockdown of Grb2 in HeLa cells, that express a low level of Cbl-b, led to a strong decrease in EGFR ubiquitination (Huang and Sorkin, 2005). In cells that have a relatively high level of Cbl-b, such as HSC3, a pool of Cbl-b, not bound to Grb2, may have a greater contribution to EGFR ubiquitination than Grb2-free pool of Cbl, assuming that the affinity and/or avidity of the direct interaction of Cbl-b with pY1045 is higher than that of Cbl.

Effects of wt and mutant Cbls on EGF-dependent EGFR degradation, signaling, and cell motility

To investigate the long-term effects of overexpression of wt Cbl/Cbl-b and their mutants on ligand-induced degradation and signaling activity of EGFR in HSC3 cells, serum-starved cells were incubated with EGF (10 ng/ml) in a large volume for up to 24 h to avoid depletion of the ligand from the medium due to endocytosis. In control cells (EV), about 50–70% and 30–50% of total EGFR protein remained after a 6-h and 24-h EGF stimulation, respectively (Figure 6, A and B), consistently with the slow turnover of EGFR in cells, such as HSC3, expressing high levels of this receptor. Overexpression of either wtCbl or wtCbl-b accelerated EGF-dependent EGFR degradation, whereas dominant-negative mutants of Cbls did not significantly affect the half-life of EGFR protein (Figure 6, A and B). The latter observation can be explained by the fact that only a fraction of EGFR (~10%; Supplemental Figure S5) is activated by 10 ng/ml EGF in HSC3 cells, and therefore, reduced EGFR ubiquitination and slower degradation of active receptors may not have a significant impact on the total receptor level. Overexpression of wtCbl and wtCbl-b also led to the decrease in the amount of active EGFR, as measured by phosphorylation of Y1068, and active ERK1/2 (Figure 6, A, C, and D). Interestingly, whereas the ΔC381_Cbl mutant did not significantly affect the amount of active EGFR, expression of the C373A_Cbl-b mutant resulted in an increased pY1068 immunoreactivity signal, indicative of a slower degradation of active EGFR in the presence of this mutant. Expression of C373A_Cbl-b however did not result in a significant increase in ERK1/2 activation (Figure 6D), which can be explained by the previous finding that a small pool of active EGFRs is sufficient for a full activation of ERK1/2 (Pinilla-Macua *et al*., 2017).

To examine the effects of overexpression of Cbl and Cbl-b mutants on EGFR-dependent cell motility, we utilized a Boyden chamber cell migration assay with EGF as chemoattractant (modified from Justus *et al*., 2014). The cells were plated on the top mesh membrane of the Transwell insert, and a number of cells migrated through 8-μm pores to the bottom surface of the insert membrane during 4 h in the absence or presence of 4 ng/ml EGF in the bottom compartment of the wells was quantified. As shown in Figure 7, EGF strongly stimulated chemotactic migration of HSC3 cells. No differences in the motility were observed between cell lines in the absence of EGF, suggesting that EGFR-independent effects of Cbl on cell adhesion and actin cytoskeleton proteins (Suetsugu *et al*., 2004; Kaabeche *et al*., 2005) do not significantly influence cell migration under these experimental conditions. In the presence of the EGF gradient, the number of migrated cells overexpressing C373A_Cbl-b was significantly lower compared with that of EV cells (Figure 7B). Numbers of migrating cells expressing ΔC381_Cbl was also lower than that of EV cells, but the trend was not statistically significant (Figure 7B).

To test whether the predominant role of Cbl-b compared with Cbl in cell motility is specific to cells expressing high levels of endogenous Cbl-b, similar EGF-chemotaxis experiments were performed in OSC-19 cells. These cells migrated towards EGF gradient, although at a much lower rate than did HSC3 cells (Figure 7C). The C373A_Cbl-b mutant had a partial migration-inhibitory effect (Figure 7, C and D), despite dramatic overexpression over endogenous Cbl-b (Supplemental Figure 3B), whereas overexpression of ΔC381_Cbl mutant virtually abolished the EGF-dependent migration of OSC-19 cells (Figure 7, C and D). These data indicate that Cbl has a greater role in the motility signaling in cells, such as OSC-19, in which Cbl-b concentration is markedly lower than that of Cbl.

The data of Figures 6 and 7 support the notion that in HSC3 cells, expressing a high Cbl-b level, inhibition of Cbl or Cbl-b individually by their dominant-negative mutants in HSC3 cells does not have a strong impact on EGFR signaling owing to largely independent mechanisms of EGFR regulation by Cbl and Cbl-b. The exception is the motility signaling in which Cbl-b appears to play a greater role in HSC3 cells. The inhibitory effect of the dominant-negative Cbl-b mutant correlates with the inhibitory effect of this mutant on the degradation of active EGFR (Figure 6C). Postendocytic traffic to late endosomes of another RTK, c-Met receptor, was proposed to be necessary for the activation of Rac1 GTPase and cell migration (Menard *et al*., 2014). Therefore, delayed endosomal sorting of active EGFR manifested in its reduced degradation may cause slow EGFR-dependent migration of cells in the presence of Cbl-b mutant. Importantly, the role of Cbl-b and Cbl in EGFR-dependent migration of HSC3 and OSC-19 cells, respectively, was demonstrated in our experiments in the presence of a near-physiological concentration of EGF (4 ng/ml), suggesting that Cbls may be involved in cell motility and invasiveness of carcinoma cells in vivo. Thus, inhibition of Cbls has the potential to be developed as a therapeutic approach for preventing metastatic growth of EGFR-dependent tumors.

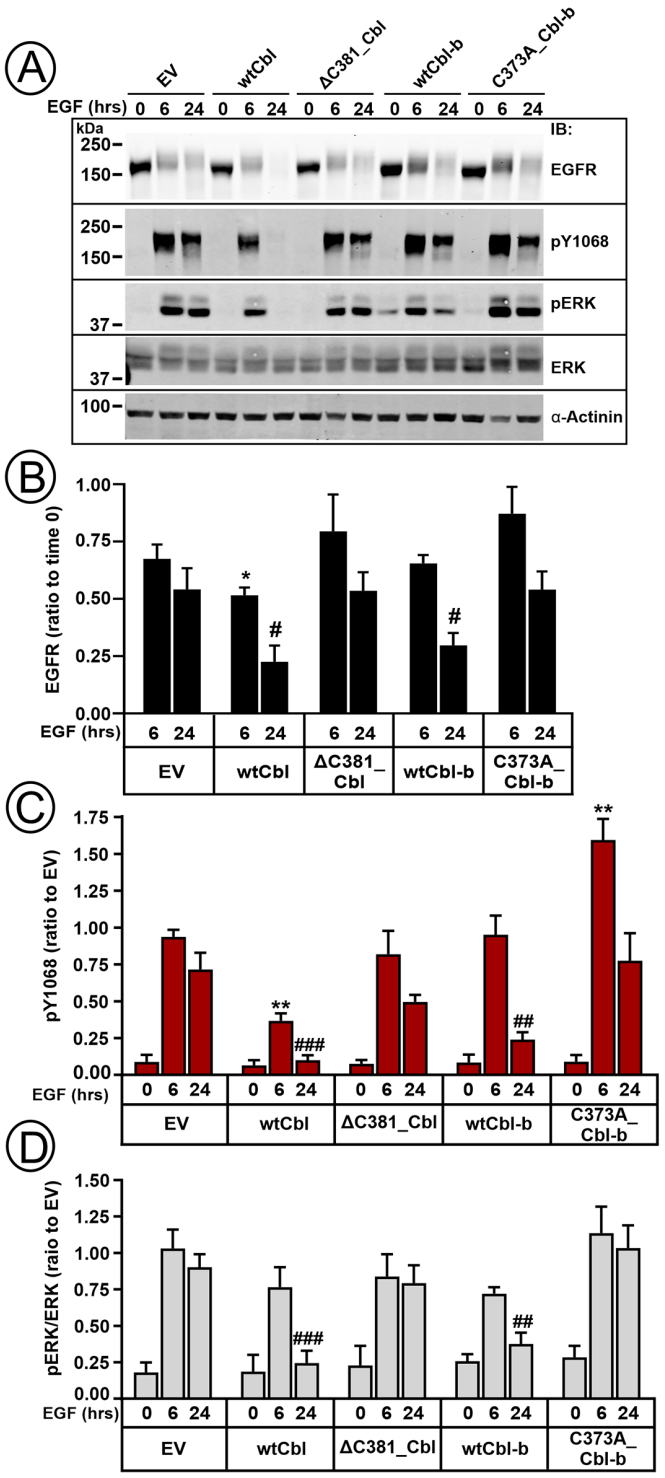

FIGURE 6: Effects of Cbls overexpression on EGFR degradation and phosphorylation, and ERK1/2 activity. HSC3 cells expressing wtCbl, wtCbl-b or their mutants were incubated with 10 ng/ml EGF for 0, 6, and 24 h in the presence of 10 μM cycloheximide. Cell lysates were probed by western blotting with antibodies to EGFR, EGFR pY1068, pERK1/2, pan-ERK1/2, and α-actinin (loading control). (A) Representative western blots. (B) Mean values of EGFR immunoreactivity normalized to α-actinin and expressed as fractions of normalized EGFR immunoreactivity at time "0" (±SEM; $n = 8$). Unpaired t tests were performed against EV for each time point. $^{*}p = 0.0468$, $^{\#}p = 0.0216$ (for wtCbl) and $p = 0.0447$ (for wtCbl-b). (C) Mean values of the pY1068 normalized to α-actinin are displayed (±SEM; $n = 8$). Unpaired t tests were performed for each time point. p values are against EV. ns, nonsignificant, $^{**}p < 0.0021$, $^{***}p < 0.0002$, $^{****}p < 0.0001$ to 6 h and $\#p < 0.0332$, $\#\#p < 0.0021$, $\#\#\#p < 0.0002$ to 24 h. (D) Mean values of pERK1/2 immunoreactivity normalized to total ERK1/2 are displayed (±SEM; $n = 8$). Unpaired t test was used for each timepoint. p values are against EV. ns nonsignificant, $^{*}p < 0.0332$, $^{**}p < 0.0021$ to 6 h and $\#\#p < 0.0021$ to 24 h. P values are not shown where differences were not statistically significant.

MATERIALS AND METHODS

Request a protocol through *Bio-protocol*.

Reagents

Recombinant human EGF was from BD Biosciences (San Jose, CA). EGF-A647 was purchased from Invitrogen (Pittsburgh, PA). Mouse monoclonal antibodies to pY1068 and pERK1/2, rabbit polyclonal antibody to α-actinin, pan-ERK1/2, and c-Cbl; and rabbit monoclonal antibody to EGFR were from Cell Signaling Technology (Danvers, MA). Mouse monoclonal antibodies to ubiquitin (P4D1), β-actin, Cbl-b were from Santa Cruz Biotechnology (Dallas, TX). Mouse monoclonal Cbl (610442) and EEA.1 antibodies were from BD Bioscience. EGFR monoclonal antibody 528 was from ATCC (Manassas, VA). Hoechst 33342 staining solution was from (Thermo Fisher Scientific, Pittsburgh, PA). Other chemicals were from Fisher Scientific or Sigma, if not indicated otherwise.

Cell Culture

HSC3 and its derivatives were maintained in Dulbecco's minimum essential medium (DMEM) supplemented with 5% fetal bovine serum (FBS). OSC-19 cells were maintained in DMEM supplemented with 10% FBS. PAE stable cell lines were maintained in F12 supplemented with 10% FBS, 2 mM L-Glutamine and Penicillin/Streptomycin. HSC3 and OSC-19 cells were authenticated by STR profiling. All cells were mycoplasma-free.

Plasmids

A lentiviral construct carrying cDNA encoding human Cbl (pSLIK-neo-Cbl vector) was provided by Dr. S. Sigismund (IFOM, Milan, Italy). pSLIK-neo ΔC381_Cbl was generated from pENT- Cbl vector by site-directed mutagenesis using QuickChange mutagenesis kit (Stratagene Cloning Systems) according to the manufacturer's protocol. The sense oligonucleotide used for ΔC381_Cbl mutant was 5′-tgtgagatgggctccacattccaactaaaaatatgtgctgaaaatgataagg-3′. pSPORT-HA-Cbl-b constructs were provided by Dr. Morag Park (McGill University, Montreal, Canada). They were subcloned into pENT vector and introduced in pSLIK-neo vector using Gateway LR Clonase (Invitrogen).

Generation of HSC3 and OSC-19 cell lines expressing Cbls and their mutants in Dox-dependent manner

The cells expressing Cbl, HA-Cbl-b and mutants under doxycycline-inducible promoter were generated using lentiviral infection. The lentiviral packaging plasmids were provided by Dr. A. Kwiatkowski (University of Pittsburgh, PA). The lentivirus stock was prepared as described (Capuani *et al.*, 2015). Cell populations stably expressing pSLIK-neo-Cbl proteins were obtained by selection on neomycin (400 μg/ml). To induce Cbl protein expression, cells were grown for 24 h, and further grown with Dox for 24 h with or without sodium butyrate (CMV promoter activator) to achieve similar levels of recombinant protein expression (wtCbl and wtCbl-b with 1 μg/ml Dox and 2 mM sodium butyrate; ΔC381_Cbl and C373A_Cbl-b mutants

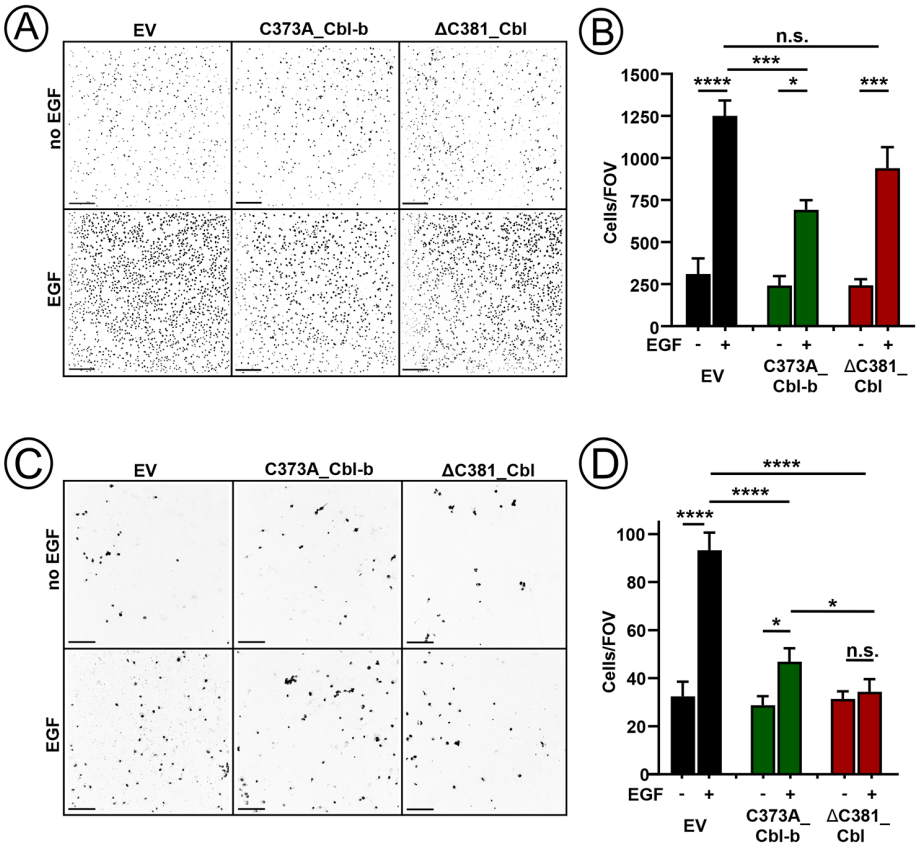

FIGURE 7: Effects of E3-activity-deficient Cbl and Cbl-b mutants on EGF-guided chemotactic motility of HSC3 and OSC-19 cells. HSC3 (A and B) or OSC-19 (C and D) Dox-on cells expressing EV, ΔC381_Cbl or C373A_Cbl-b mutants were plated in the upper chamber of pretreated Transwell inserts (10^5 cells/insert). Media with or without 4 ng/ml EGF was added to the bottom compartment of wells. Cells were incubated for 4 h at 37°C to allow cell migration to the bottom surface of Transwell inserts, fixed and nuclei were stained with Hoescht 33342. Nuclei of cells on the bottom surface of Transwell inserts were imaged through the 405-nm (*blue*) channel. (A and C) Examples of FOV images. Images are shown in inverted black-and-white mode. Scale bars, 200 μm. (B and D) Bar graphs represent mean values of number of cells per FOV (±SEM; six FOVs per experiment; $n = 4–5$ of independent experiments). One-way ANOVA test was performed. *$p < 0.0332$, **$p < 0.0021$, ***$p < 0.0002$, ****$p < 0.0001$; ns, not significant.

with 1 μg/ml Dox; and ΔUBA_Cbl-b with 0.32 μg/ml Dox) followed by experimental manipulations. Clonal pools carrying an empty pSLIK-neo vector (EV) were obtained in parallel and used as an experimental control.

RNAi interference

Grb2 (Jiang *et al.*, 2003), c-Cbl and Cbl-b (Huang *et al.*, 2006) siRNA duplexes were resuspended in 1 × siRNA universal buffer (Dharmacon, Lafayette, Colorado) to 20 μM before transfection. Nontargeting siRNA was from Qiagen. Parental and derived cell lines grown in 60-mm dishes (60–80% confluency) were transfected with siRNA duplexes at a final concentration of 100 nM with DharmaFECT I reagent (Dharmacon) following manufacturer's protocol. After 24 h, the cells were replated to 100-mm dishes and used for experiments 2 d after.

EGFR immunoprecipitation and western blotting

Serum-starved cells were stimulated with EGF for 15 min at 37°C unless otherwise stated, washed with ice-cold Ca^{2+}, Mg^{2+}-free PBS and lysed in Triton X-100-glycerol-HEPES (TGH) buffer (1% Triton X-100, 10% (vol/vol) glycerol, 50 mM HEPES, 50 mM NaCl, 1 mM EDTA, 10 mM n-ethylmaleimide, 1 mM orthovanadate, and other phosphatase and protease inhibitors) as described in (Pinilla-Macua *et al.*, 2016). Lysates were cleared by centrifugation and used for EGFR immunoprecipitation (1–1.5 mg protein) with the antibody 528 (10 μg/sample).

The immunoprecipitates and aliquots of lysates (100 μg protein) were resolved by SDS–PAGE (7.5 and 10% gels, respectively), followed by the transfer to the nitrocellulose membrane. Western blotting was performed by incubating with appropriate primary antibodies followed by secondary antibodies conjugated to far-red fluorescent dyes (IRDye-680 and -800) and detection using an Odyssey Li-COR system. Quantifications were performed using Li-COR software.

For examining effects of Cbls overexpression on EGFR degradation and signaling, HSC3 derived cells grown with doxycycline (±sodium butyrate) were preincubated with 10 μM cycloheximide for 30 min in DMEM supplemented with 0.1% bovine serum albumin (BSA). The cells were then incubated in DMEM containing 0.1% BSA with 10 ng/ml EGF in the presence of 10 μM cycloheximide for 0, 6, and 24 h at 37°C. Cells were lysed in TGH buffer and precleared lysates (100 μg protein) were resolved by SDS–PAGE and transferred to the nitrocellulose membrane. Western blotting and quantifications were performed as described above.

Measurement of EGFR internalization rates using ^{125}I-EGF

Mouse receptor-grade EGF (Collaborative Research) was iodinated as described (Sorkin and Duex, 2010). The cells were incubated with ^{125}I-EGF (1 ng/mL) for 1-5 min at 37°C. The time–course of ^{125}I-EGF internalization was used to calculate the specific internalization rate constant K_e as the linear regression coefficient of the dependence of the ratio of internalized/surface ^{125}I-EGF on time as described (Sorkin and Duex, 2010). The low concentration of ^{125}I-EGF and short incubation times were used to avoid saturation of the CME pathway and minimize contribution of recycling, respectively.

Fluorescence microscopy

The cells were grown on glass coverslips. After incubation with EGF-Rh or EGF-A647 (4 ng/ml), the cells were washed in PBS and fixed in freshly prepared 4% paraformaldehyde (PFA). Fixed cells were permeabilized with 0.1%Triton X-100 for 10 min, blocked in 3% BSA/PBS for 30 min at room temperature (RT) and incubated with c-Cbl (mAb), Cbl-b, EEA1, or EGFR as primary antibodies for 1 h at RT. Cells were then incubated with secondary antibodies for 1 h at RT. The nuclei were stained with Hoechst 33342 during incubation with secondary antibodies. Cells were mounted in ProLong Gold.

Z-stack of *x-y* confocal images were acquired using a Marianas spinning disk confocal imaging system based on Zeiss Axio Observer

Z1 inverted fluorescence microscope system equipped with 63× Plan Apo PH NA1.4 objective, and controlled by SlideBook 6 software (Intelligent Imaging Innovation, Denver, CO) as described (Perez Verdaguer *et al.*, 2021). All image acquisition settings were identical for all experimental variants in each experiment.

To quantify the fraction of EGF-Rh in early/sorting endosomes in immunofluorescence experiments, a segment mask (EGF Mask) was created from background-subtracted three-dimensional images to select all voxels positive for 561-nm fluorescence using the same low-intensity threshold in all variants of each experiment. EEA1 was detected using secondary antibodies conjugated with Cy5. Therefore, EEA1 Mask was generated to select voxels positive for 640-nm channel fluorescence using the same low-intensity threshold in all variants. Finally, the sum fluorescence intensity through 561-nm channel in the EEA1 Mask was divided to that intensity in the EGF Mask to calculate the percent of EGF-Rh colocalized with EEA1 of total cell-associated EGF-Rh per a field of view (FOV).

To quantify the ratio of the amounts of Cbls and EGF-A647 in endosomes in immunofluorescence experiments, a segment Mask one was created to select vesicles positive for 640-nm fluorescence using the same low-intensity threshold in all variants of each experiment. In cells incubated with EGF-A647 for 15 min, Mask1 predominantly selects endosomes containing EGF-A647:EGFR complexes because of their high intensity of EGF-A647 fluorescence compared with that of the plasma membrane and vesicular autofluorescence. Mask two was generated to select voxels positive for Cbls (561-nm channel fluorescence) using the same low-intensity threshold in all variants for each Cbl protein. Mask three was generated to contain voxels common in Masks one and two, and thus containing both EGF-A647 and Cbls. Mask four was created by dilation of individual objects in Mask three by two voxels in three dimensions, and Mask three was subtracted from Mask four to generate the background mask (BackMask) for objects in Mask three. Finally, mean fluorescence intensities of 561-nm and 640-nm channels of BackMask in individual cells were subtracted from those intensities in Mask three. The ratio of these intensities corresponding to the ratio of Cbl or Cbl-b to EGF-A647 in endosomes was then calculated per individual cell.

Boyden chamber cell migration assays

HSC3 and OSC-19 derived cells were grown with Dox (–/+ sodium butyrate) to induce expression. Transwell inserts (8-μm pore size, Polycarbonate membrane, Corning) were placed into the wells of 24-well plates. The bottom surface of the insert membrane was coated with 50 μg/ml fibronectin (Sigma/Millipore) in PBS. Serum-starved cells were plated into the insert (10^5 cell/well) in DMEM containing 0.1% BSA. To assess cell migration in the presence of the chemoattractant (EGF) gradient, lower compartment of wells contained 600 μl of DMEM/0.1% BSA with or without 4 ng/ml EGF. After 4 h, inserts were fixed in 4% PFA, and cells remaining in the upper compartment were removed using cotton swabs. The nuclei of cells migrated through pores to the bottom side of the insert membrane were stained with Hoechst 33342 for 15 min. Membranes were air-dried prior imaging using a Marianas spinning disk confocal system and 10× air NA 0.3 objective through the 405-nm laser channel. To count migrated cells, a segment mask was generated to select Hoechst 33342 positive objects representing nuclei of migrated cells. Six individual FOV were captured for each biological replicate, and mean numbers of cells per FOV was calculated. Identical image acquisition and analysis parameters were used in all variants in each experiment.

Statistical data analysis

Statistical analysis was performed using GraphPad Prism version 7.0 (La Jolla California). One-way ANOVA to control and unpaired *t* test comparing each experimental group to control were normally used. Differences were considered significant if p values are <0.05. p values and numbers of biological replicates are indicated in Figure Legends.

ACKNOWLEDGMENTS

We are grateful to Adam Kwiatkowski, Morag Park and Sara Sigismund for the gifts of reagents. Supported by National Institutes of Health grants - GM148363 and CA089151.

REFERENCES

Baycin-Hizal D, Tabb DL, Chaerkady R, Chen L, Lewis NE, Nagarajan H, Sarkaria V, Kumar A, Wolozny D, Colao J, *et al*. (2012). Proteomic analysis of Chinese hamster ovary cells. J Proteome Res 11, 5265–5276.

Capuani F, Conte A, Argenzio E, Marchetti L, Priami C, Polo S, Di Fiore PP, Sigismund S, Ciliberto A (2015). Quantitative analysis reveals how EGFR activation and downregulation are coupled in normal but not in cancer cells. Nat Commun 6, 7999.

Cho NH, Cheveralls KC, Brunner A-D, Kim K, Michaelis AC, Raghavan P, Kobayashi H, Savy L, Li JY, Canaj H, *et al*. (2022). OpenCell: Endogenous tagging for the cartography of human cellular organization. Science 375, eabi6983.

Crotchett BLM, Ceresa BP (2021). Knockout of c-Cbl slows EGFR endocytic trafficking and enhances EGFR signaling despite incompletely blocking receptor ubiquitylation. Pharmacol Res Perspect 9, e00756.

Davies GC, Ettenberg SA, Coats AO, Mussante M, Ravichandran S, Collins J, Nau MM, Lipkowitz S (2004). Cbl-b interacts with ubiquitinated proteins; differential functions of the UBA domains of c-Cbl and Cbl-b. Oncogene 23, 7104–7115.

de Poorter JJ, Lipinski KS, Nelissen RG, Huizinga TW, Hoeben RC (2007). Optimization of short-term transgene expression by sodium butyrate and ubiquitous chromatin opening elements (UCOEs.). J Gene Med 9, 639–648.

Duan L, Miura Y, Dimri M, Majumder B, Dodge IL, Reddi AL, Ghosh A, Fernandes N, Zhou P, Mullane-Robinson K, *et al*. (2003). Cbl-mediated ubiquitinylation is required for lysosomal sorting of epidermal growth factor receptor but is dispensable for endocytosis. J Biol Chem 278, 28950–28960.

Eden ER, Huang F, Sorkin A, Futter CE (2012). The role of EGF receptor ubiquitination in regulating its intracellular traffic. Traffic 13, 329–337.

Ettenberg SA, Keane MM, Nau MM, Frankel M, Wang LM, Pierce JH, Lipkowitz S (1999). cbl-b inhibits epidermal growth factor receptor signaling. Oncogene 18, 1855–1866.

Ettenberg SA, Magnifico A, Cuello M, Nau MM, Rubinstein YR, Yarden Y, Weissman AM, Lipkowitz S (2001). Cbl-b-dependent coordinated degradation of the epidermal growth factor receptor signaling complex. J Biol Chem 276, 27677–27684.

Fortian A, Dionne LK, Hong SH, Kim W, Gygi SP, Watkins SC, Sorkin A (2015). Endocytosis of ubiquitylation-deficient EGFR mutants via Clathrin-coated pits is mediated by ubiquitylation. Traffic 16, 1137–1154.

Goh LK, Huang F, Kim W, Gygi S, Sorkin A (2010). Multiple mechanisms collectively regulate clathrin-mediated endocytosis of the epidermal growth factor receptor. J Cell Biol 189, 871–883.

Goh LK, Sorkin A (2013). Endocytosis of receptor tyrosine kinases. Cold Spring Harb Perspect Biol 5, a017459.

Grovdal LM, Stang E, Sorkin A, Madshus IH (2004). Direct interaction of Cbl with pTyr 1045 of the EGF receptor (EGFR) is required to sort the EGFR to lysosomes for degradation. Exp Cell Res 300, 388–395.

Huang F, Kirkpatrick D, Jiang X, Gygi S, Sorkin A (2006). Differential regulation of EGF receptor internalization and degradation by multiubiquitination within the kinase domain. Mol Cell 21, 737–748.

Huang F, Sorkin A (2005). Growth factor receptor binding protein 2-mediated recruitment of the RING domain of Cbl to the epidermal growth factor receptor is essential and sufficient to support receptor endocytosis. Mol Biol Cell 16, 1268–1281.

Jiang X, Huang F, Marusyk A, Sorkin A (2003). Grb2 regulates internalization of EGF receptors through clathrin-coated pits. Mol Biol Cell 14, 858–870.

Jiang X, Sorkin A (2003). Epidermal growth factor receptor internalization through clathrin-coated pits requires Cbl RING finger and proline-rich domains but not receptor polyubiquitylation. Traffic 4, 529–543.
Justus CR, Leffler N, Ruiz-Echevarria M, Yang LV (2014). In vitro cell migration and invasion assays. J Vis Exp 88, 51046.
Kaabeche K, Guenou H, Bouvard D, Didelot N, Listrat A, Marie PJ (2005). Cbl-mediated ubiquitination of alpha5 integrin subunit mediates fibronectin-dependent osteoblast detachment and apoptosis induced by FGFR2 activation. J Cell Sci 118, 1223–1232.
Kozlov G, Peschard P, Zimmerman B, Lin T, Moldoveanu T, Mansur-Azzam N, Gehring K, Park M (2007). Structural basis for UBA-mediated dimerization of c-Cbl ubiquitin ligase. J Biol Chem 282, 27547–27555.
Kulak NA, Pichler G, Paron I, Nagaraj N, Mann M (2014). Minimal, encapsulated proteomic-sample processing applied to copy-number estimation in eukaryotic cells. Nat Methods 11, 319–324.
Lemmon MA, Schlessinger J (2010). Cell signaling by receptor tyrosine kinases. Cell 141, 1117–1134.
Levkowitz G, Waterman H, Ettenberg SA, Katz M, Tsygankov AY, Alroy I, Lavi S, Iwai K, Reiss Y, Ciechanover A, *et al*. (1999). Ubiquitin ligase activity and tyrosine phosphorylation underlie suppression of growth factor signaling by c-Cbl/Sli-1. Mol Cell 4, 1029–1040.
Menard L, Parker PJ, Kermorgant S (2014). Receptor tyrosine kinase c-Met controls the cytoskeleton from different endosomes via different pathways. Nat Commun 5, 3907.
Mitra P, Zheng X, Czech MP (2004). RNAi-based analysis of CAP, Cbl, and CrkII function in the regulation of GLUT4 by insulin. J Biol Chem 279, 37431–37435.
Ohnishi Y, Lieger O, Attygalla M, Iizuka T, Kakudo K (2008). Effects of epidermal growth factor on the invasion activity of the oral cancer cell lines HSC3 and SAS. Oral Oncol 44, 1155–1159.
Ohno A, Ochi A, Maita N, Ueji T, Bando A, Nakao R, Hirasaka K, Abe T, Teshima-Kondo S, Nemoto H, *et al*. (2016). Structural analysis of the TKB domain of ubiquitin ligase Cbl-b complexed with its small inhibitory peptide, Cblin. Arch Biochem Biophys 594, 1–7.
Pastore S, Mascia F, Mariani V, Girolomoni G (2008). The epidermal growth factor receptor system in skin repair and inflammation. J Invest Dermatol 128, 1365–1374.
Pennock S, Wang Z (2008). A tale of two Cbls: interplay of c-Cbl and Cbl-b in epidermal growth factor receptor downregulation. Mol Cell Biol 28, 3020–3037.
Perez Verdaguer M, Zhang T, Paulo JA, Gygi S, Watkins SC, Sakurai H, Sorkin A (2021). Mechanism of p38 MAPK-induced EGFR endocytosis and its crosstalk with ligand-induced pathways. J Cell Biol 220, e202102005.
Peschard P, Kozlov G, Lin T, Mirza IA, Berghuis AM, Lipkowitz S, Park M, Gehring K (2007). Structural basis for ubiquitin-mediated dimerization and activation of the ubiquitin protein ligase Cbl-b. Mol Cell 27, 474–485.
Pinilla-Macua I, Grassart A, Duvvuri U, Watkins SC, Sorkin A (2017). EGF receptor signaling, phosphorylation, ubiquitylation and endocytosis in tumors in vivo. eLife 6, e31993.
Pinilla-Macua I, Watkins SC, Sorkin A (2016). Endocytosis separates EGF receptors from endogenous fluorescently labeled HRas and diminishes receptor signaling to MAP kinases in endosomes. Proc Natl Acad Sci USA 113, 2122–2127.
Rao N, Dodge I, Band H (2002). The Cbl family of ubiquitin ligases: critical negative regulators of tyrosine kinase signaling in the immune system. J Leukoc Biol 71, 753–763.
Rorsman C, Tsioumpekou M, Heldin CH, Lennartsson J (2016). The ubiquitin ligases c-Cbl and Cbl-b negatively regulate platelet-derived growth factor (PDGF) BB-induced chemotaxis by affecting PDGF receptor beta (PDGFRbeta) internalization and signaling. J Biol Chem 291, 11608–11618.
Schmidt MH, Dikic I (2005). The Cbl interactome and its functions. *Nature reviews*. Mol Cell Biol 6, 907–918.
Sibilia M, Kroismayr R, Lichtenberger BM, Natarajan A, Hecking M, Holcmann M (2007). The epidermal growth factor receptor: from development to tumorigenesis. Differentiation 75, 770–787.
Sigismund S, Algisi V, Nappo G, Conte A, Pascolutti R, Cuomo A, Bonaldi T, Argenzio E, Verhoef LG, Maspero E, *et al*. (2013). Threshold-controlled ubiquitination of the EGFR directs receptor fate. EMBO J 32, 2140–2157.
Sorkin A, Duex JE (2010). Quantitative analysis of endocytosis and turnover of epidermal growth factor (EGF) and EGF receptor. Curr Protoc Cell Biol Chapter 15:Unit 15.14.
Sorkin A, Goh LK (2009). Endocytosis and intracellular trafficking of ErbBs. Exp Cell Res 315, 683–696.
Suetsugu S, Tezuka T, Morimura T, Hattori M, Mikoshiba K, Yamamoto T, Takenawa T (2004). Regulation of actin cytoskeleton by mDab1 through N-WASP and ubiquitination of mDab1. Biochem J 384, 1–8.
Swaminathan G, Tsygankov AY (2006). The Cbl family proteins: ring leaders in regulation of cell signaling. J Cell Physiol 209, 21–43.
Thien CB, Langdon WY (2005). c-Cbl and Cbl-b ubiquitin ligases: substrate diversity and the negative regulation of signalling responses. Biochem J 391, 153–166.
Uribe ML, Marrocco I, Yarden Y (2021). EGFR in cancer: signaling mechanisms, drugs, and acquired resistance. Cancers (Basel) 13, 2748.
von Zastrow M, Sorkin A (2021). Mechanisms for regulating and organizing receptor signaling by endocytosis. Annu Rev Biochem 90, 709–737.
Waterman H, Katz M, Rubin C, Shtiegman K, Lavi S, Elson A, Jovin T, Yarden Y (2002). A mutant EGF-receptor defective in ubiquitylation and endocytosis unveils a role for Grb2 in negative signaling. EMBO J 21, 303–313.
Waterman H, Levkowitz G, Alroy I, Yarden Y (1999). The RING finger of c-Cbl mediates desensitization of the epidermal growth factor receptor. J Biol Chem 274, 22151–22154.
Xu H, Stabile LP, Gubish CT, Gooding WE, Grandis JR, Siegfried JM (2011). Dual blockade of EGFR and c-Met abrogates redundant signaling and proliferation in head and neck carcinoma cells. Clin Cancer Res 17, 4425–4438.
Yokoi T, Yamaguchi A, Odajima T, Furukawa K (1988). Establishment and characterization of a human cell line derived fron a squamous carcinoma of the tongue. Tumor Res 23, 43–57.